Int. J. Heat Mass Transfer. Vol. 31, No. 2, pp. 331–348, 1988
Printed in Great Britain

0017–9310/88 $3.00 + 0.00

An experimental study of natural convection effects on downward freezing of pure water

R. A. BREWSTER and B. GEBHART

Department of Mechanical Engineering and Applied Mechanics, University of Pennsylvania, Philadelphia, PA 19104, U.S.A.

(*Received* 31 *August* 1987)

Abstract—Measurements of ice freezing downward into a quiescent deep pure water layer are presented. This occurs in processing and also on terrestrial water surfaces. The coupled mechanisms of convection and freezing were shown to be very complicated, due both to the buoyancy force reversals characteristic of cold water thermal transport and major liquid supercooling. Previous comparable studies have been limited to small and very confined geometries. The present larger scale measurements determined both freezing and convective heat transfer rates. Non-freezing measurements were also made, to characterize the purely convective effects. Time-exposure visualizations of typical flows are given for ambient water temperatures in the range of 1–9°C. The density anomaly in cold water has very large effects on both the flows and freezing rates. Large liquid supercooling always preceded initial freezing. Resulting transient changes in the buoyancy force were found to have large effects under many conditions. Measurements of ice thicknesses and cooling surface temperatures are used to calculate heat transfer coefficients and ice growth 'efficiencies'. These measurements provide detailed quantitative insight into the relative roles of supercooling, freezing and natural convection in the downward growth processes of horizontal ice surfaces in cold water.

1. INTRODUCTION

ICE GROWTH characteristics are important in many technological and geophysical circumstances. Technological applications include water desalination, ice production, and the understanding of crystal growth processes. In oceans and lakes, ice forms on the water surface, growing downward into a deep water layer. Natural convection in the unfrozen liquid usually plays a vital role in determining the rate of ice growth. The anomalous behavior of the water density near 4°C further complicates matters. Buoyancy force reversals arise across temperature gradients in low temperature water.

Investigations of natural convection flows in cold water abound in the literature. These were most recently reviewed in ref. [1]. In particular, many studies had appeared concerning the convective motions associated with ice melting in pure and saline water, as described in ref. [2]. An important feature of such flows is the existence of a minimum heat transfer and/or melting rate in pure water near 5.5°C. This arises as competing buoyancy force effects result in very weak convective motions.

Previous studies of the role of natural convection in solidification processes have mostly been in very confined geometries. An early study, by Thomas and Westwater [3], used n-octadecane as the test fluid. Observations were made of the phase boundary velocity for freezing in a 3/8 × 1/2 × 2 in. high test cell. Boger and Westwater [4] made measurements of interfacial velocities and transient and steady-state temperature profiles during the freezing and melting of pure water in a 0.5 × 0.5 × 2.0 in. high test chamber. Freezing or melting was initiated from either above or below. At high Rayleigh numbers, oscillations in the interface velocity were observed.

Foster [5] visualized the freezing of sea water from above. In this circumstance, both thermal and mass diffusion are present during freezing. The test chamber had inside dimensions of 25 × 25 × 25 cm. The flow was visualized using a schlieren optical system. For salinities between 20 and 24.7‰, no convection was observed before freezing and significant supercooling of the liquid occurred. When freezing did occur, a thick layer of ice formed within a few seconds. Then convection began in the form of downward plunging sheets. For salinities greater than 24.7‰, significant supercooling did not occur, but convection began before freezing.

Tankin and Farhadieh [6] used a Mach–Zehnder interferometer to study the formation of ice from pure water. The test section measured 2.5 × 2.75 × 0.75 in. high. Freezing was initiated from above or from below. A layer of supercooled water was observed adjacent to the cooling surface, then dendritic ice formed suddenly, extending to the 0°C isotherm. Farhadieh and Tankin [7, 8] later extended these observations to the freezing of sea water. The temperature of the water–ice interface was reported to be 0°C, rather than the saline water equilibrium freezing temperature.

One-dimensional freezing of sodium chloride solutions from above has been investigated by Grange *et al.* [9, 10] using a Mach–Zehnder interferometer. In the former study, the test section measured

NOMENCLATURE

A	area of aluminum cooling surface
B	$(\rho_\infty - \rho_0)/\rho_m$
E_{ice}	$(Q_{ice}/Q_B) \times 100$
$h(\tau)$	heat transfer coefficient
h_{il}	specific heat of fusion of water
q''_B	heat flux through bottom of aluminum cooling surface
$\overline{q''_{B,BF}}$	integrated average of q''_B over time before freezing
q''_{conv}	heat flux transferred by convection
q''_{ice}	$\rho_{ice} h_{il} (d\delta/d\tau)$
Q_B	total heat transferred through aluminum cooling surface during experiment
Q_{ice}	$A\rho_{ice} h_{il} \delta(\tau = 30 \text{ min})$
$R(\tau)$	$(t_m - t_\infty)/(t_0 - t_\infty)$
R_{ice}	$(t_m - t_\infty)/(t_{il} - t_\infty)$
R_{msc}	$(t_m - t_\infty)/(t_{msc} - t_\infty)$
t	temperature
t_B	temperature at bottom of aluminum cooling surface
t_{il}	equilibrium freezing temperature of water, 0°C
t_{msc}	maximum supercooling temperature at the cooling surface
Δt_{TB}	temperature change at tank bottom
U_c	characteristic velocity.

Greek symbols

δ	ice thickness
ρ	fluid density
ρ_{ice}	ice density
τ	time
τ_{ice}	time at which initial ice formation occurs.

Subscripts

m	value at the density extremum
0	relevant surface value
∞	value in the ambient.

Superscript

$\overline{\ }$	average quantity.

3.75 × 2.35 × 6.1 cm high, while in the latter study a 2.75 × 2.28 × 6.1 cm test section was used. Convection in the form of 'salt fingers' was observed. At later times, a layer of high solute concentration liquid formed at the bottom of the test cell. This layer was seen to be stable despite an adverse temperature gradient.

Gau and Viskanta [11] visualized the mechanisms of freezing n-octadecane from above in a rectangular cavity measuring 6.35 × 3.81 × 8.89 cm high. Aluminum powder was used as a flow tracer. At early times, thermals fell from the cooled surface. Later on, two-dimensional rolls arose. The solid–liquid interface was seen to be flat initially, and later concave to the solid.

Most recently, Nishimura *et al.* [12] studied the freezing of pure water in test sections measuring 8.0 × 3.0 × 13.0 cm high and 38.0 × 3.0 × 10.0 cm high. Freezing was initiated from either the top or the bottom. Appreciable natural convection effects caused a nearly uniform temperature throughout the liquid phase. Finite-element solutions, assuming a uniform liquid temperature, yielded good agreement with the experimental data.

The results reported here concern the heat transfer and fluid flow processes associated with the downward freezing of an ice surface into a deep layer of pure water. The convective motions were visualized and the freezing rates determined over an ambient water temperature range of 1–9°C. Many changing and complex features of flow were seen over this range, which spans that of buoyancy force reversal. Large water supercooling was measured under many temperature conditions and levels of abstracted heat flux. The accompanying temperature and ice thickness measurements permitted the determination of the relative importance of natural convection in the water, on the ice growth process.

2. EXPERIMENT

A schematic of the experiment is shown in Fig. 1. Water in a 20 gallon hexagonal glass tank (22 in. high × 9 in. wide per hexagonal side) is cooled from above. The cooling surface is a 4.28 × 4.28 in. aluminum block (1.08 in. thick). Four Melcor CP5-31-10L thermoelectric cooling modules (TCMs), each measuring 2.14 × 2.14 in., are bonded to the top of the aluminum block. These modules are solid state heat pumps. The TCMs transfer heat from the aluminum block to ethylene glycol circulating through a copper block bonded to the top of the TCMs. Omegatherm 201 conductive paste was used to ensure good thermal contact between the TCMs and the copper and aluminum blocks. The heat flux through the cooling system is dependent upon the power supplied to the TCMs.

The tank was filled with deionized water having an electrical resistivity between 0.1 and 0.5 MΩ cm. The resistivity was periodically checked and the water replaced when found to be outside of the above-mentioned range. The tank was insulated on all sides with 1 in. thick polystyrene insulation. Teflon covered polystyrene insulation was used to insulate the exposed water surface around the aluminum block.

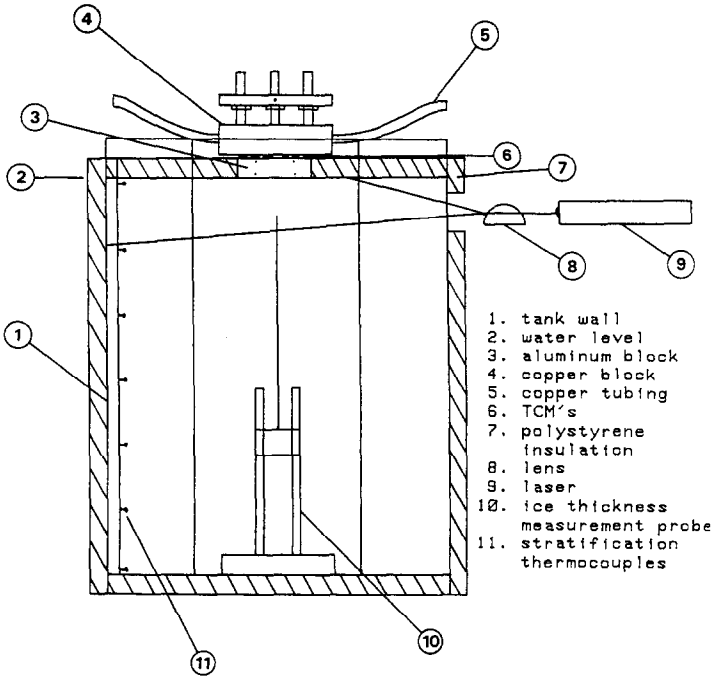

FIG. 1. Schematic of experimental apparatus.

Eight copper–constantan thermocouples, one each at the top and bottom of each of the four cooling quadrants in the aluminum block, monitored temperatures in the block. A vertical array of seven evenly spaced thermocouples measured water temperatures at various water depths. The data acquisition system was a Hewlett–Packard 3497A scanner, 3456A digital voltmeter and 9845B computer.

The entire experiment was contained in a large cold room which may be maintained at temperatures between -30 and 20°C. The desired water temperature was obtained by allowing sufficient time for the water temperature to equilibrate with the set cold room temperature.

The flow visualization consisted of time-exposure photographs of illuminated 40 μm pliolite particles suspended in the water. Pliolite is a solid white resin which is virtually insoluble in water and has a specific gravity of 1.026. A beam from a 7.0 mW helium–neon laser was spread by a lens into a vertical curtain, perpendicular to the plane of the cooling surface. The curtain was at the mid-span of the aluminum block. Scatter by the pliolite particles made them visible. A 35 mm camera took time-exposure photographs of the particles, from a small angle below, as they were moved by the buoyancy-induced flow. The exposure times and interval times between photographs were controlled by an intervalometer.

Before each experiment, the tank water was stirred for several minutes to evenly distribute the pliolite particles and to eliminate any initial temperature differences. A period of 30–60 min was then allowed for the damping of the fluid motions by viscosity.

When the experiment was begun, a running clock was started. For experiments in which ice formed, the ice thickness was measured every 2–3 min by a probe raised from the bottom of the tank. The time for each measurement was recorded using the running clock. Each experiment was 30 min long.

3. FLOW VISUALIZATION

The qualitative nature of the various flow regimes due to the density inversion effect, depending upon the ambient water temperature t_∞, may be understood from Fig. 2. Assuming that ice exists on the cooling surface and that the water–ice interface is at the equilibrium freezing temperature $t_{il} = 0$°C, there are three distinct regimes in Fig. 2(a). The first of these, region I, corresponds to $0 \leqslant t_\infty \leqslant 4$°C. In this regime, the buoyancy force is everywhere upward. Since the cooling surface is downward facing and horizontal, this represents a stably stratified circumstance. Region II is the ambient temperature range $4 \leqslant t_\infty \leqslant 8$°C. The buoyancy force is negative in the bottom region of the cooled water layer. In an analytical study of buoyancy-induced flows adjacent to horizontal surfaces in cold water, ref. [13] predicts 'convective inversion' in region II for $t_\infty \simeq 5.7$°C. In region III, $t_\infty \geqslant 8$°C, all of the fluid in the cooled layer is more dense than the ambient fluid. Therefore, the buoyancy force is everywhere downward.

In general, the water temperature and the surface temperature define the flow regime. The above range of possibilities is quantified by the instantaneous parameter $R(\tau)$, defined as

$$R(\tau) = \frac{t_m - t_\infty}{t_0(\tau) - t_\infty} \tag{1}$$

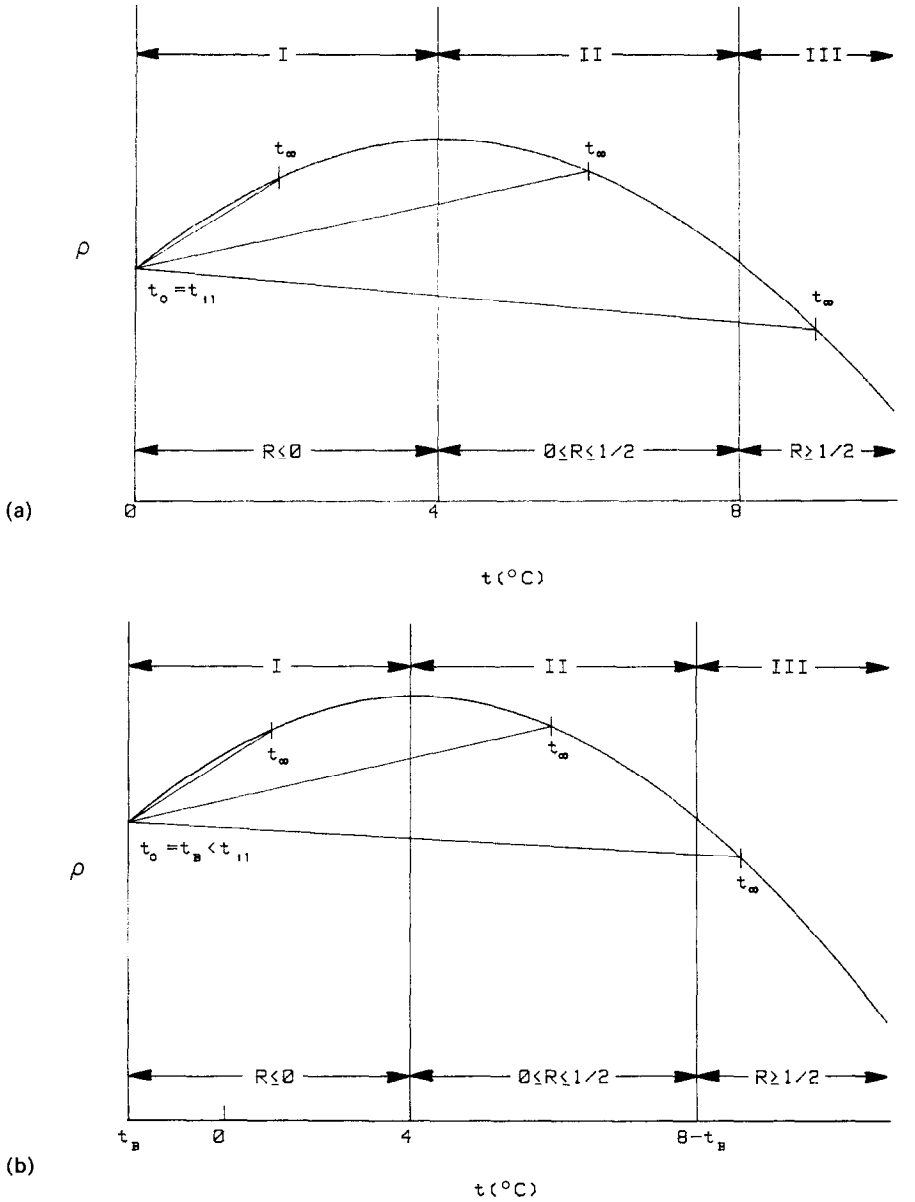

FIG. 2. Density variation of cold water showing the relation of R to t_∞ when: (a) ice is present, $t_0 = t_{il} = 0°C$; (b) supercooling occurs, $t_0 = t_B < t_{il} = 0°C$.

where the maximum density temperature is $t_m = 4.029°C$, according to the density correlation of ref. [14]. The plate or ice surface temperature is t_0, and τ is time. When no ice is present, the surface temperature is $t_0 = t_B$, where t_B is the temperature at the bottom of the aluminum cooling block. Since t_B is in general a function of time, R also changes with time. After freezing begins, $t_0 \approx t_{il}$.

Regions I, II and III correspond to $R \leqslant 0$, $0 \leqslant R \leqslant 1/2$, and $R \geqslant 1/2$, respectively. However, the three regimes as defined by the ranges of R given above are not in general restricted to any particular value of the surface temperature t_0.

Thermal stability of a horizontal layer of cold water between isothermal plates has been examined by Mollendorf and Jahn [15]. The relevant regimes for thermal stability in terms of R as defined above, are: $R \leqslant 0$ (stable), $0 \leqslant R \leqslant 1$ (locally unstable) and $R \geqslant 1$ (unstable). However, the mechanisms of thermal instability are not as important in this study because convective motion begins long before the critical Rayleigh number for thermal instability is reached in the transient. Therefore, lateral effects dominate.

3.1. *Region* I: $R \leqslant 0$

Visualizations for an experiment at $t_\infty = 0.9°C$ are shown in Fig. 3. The aluminum cooling surface is at the top-center of each photograph. The curtain of light is seen at the mid-span of the aluminum block. This location is shown as a bright straight line across the underside of the block. In all of the experiments

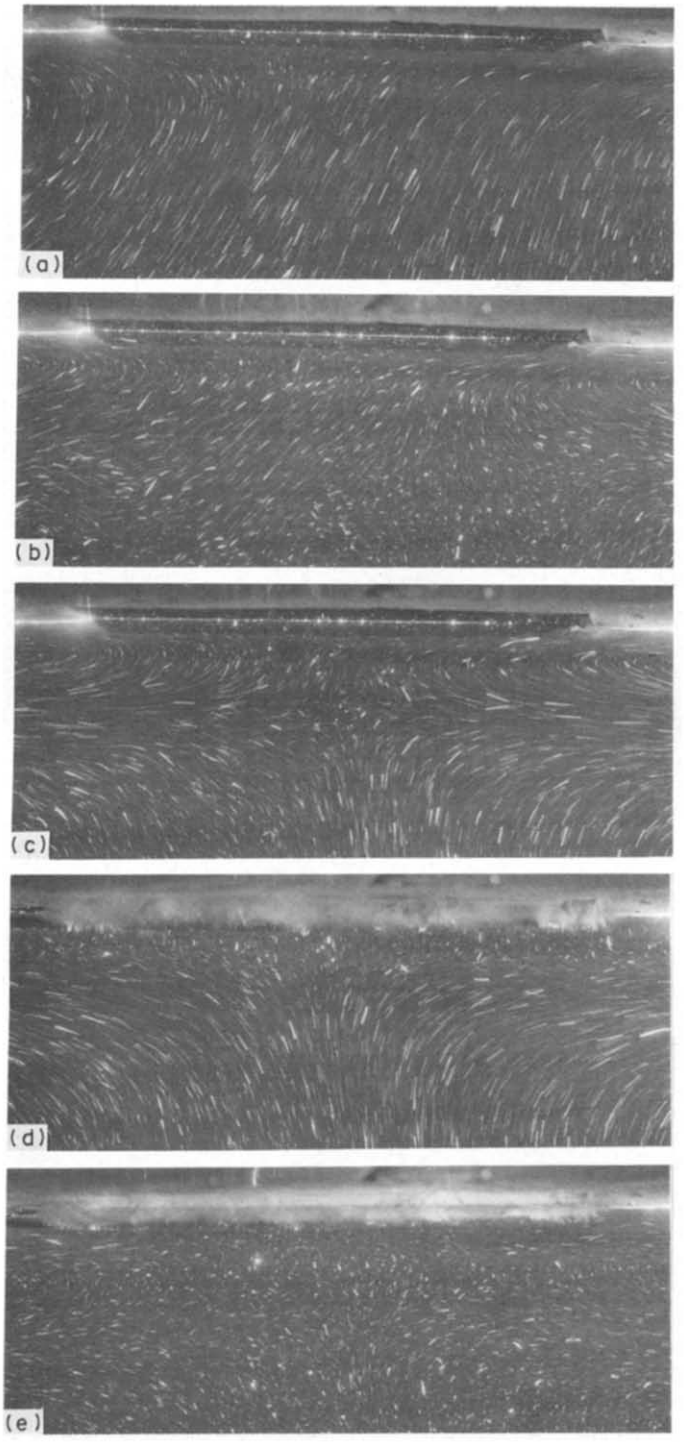

FIG. 3. Flow visualization for $t_\infty = 0.9°C$ and $\overline{q''}_{B,BF} = 686$ W m^{-2}. Exposure durations in seconds, effective surface temperature, and R's are: (a) 220–280, $-2.7°C$, -0.87; (b) 1020–1080, $-4.5°C$, -0.58; (c) 1260–1320, $-4.6°C$, -0.57; (d) 1340–1400, $0°C$, -3.48; (e) 1580–1640, $0°C$, -3.48.

Table 1. Data for 21 representative experiments

Exp.	t_∞ (°C)	$\overline{q''_{B,BF}}$ (W m^{-2})	τ_{ice} (min)	t_{msc} (°C)	E_{ice} (%)	Δt_{TB} (°C)
1	0.8	577	—	−4.1	0	0.1
2	0.9	685	22.5	−4.6	37.0	0.1
3	1.1	966	12.25	−5.7	51.3	0.0
4	1.8	637	—	−3.8	0	0.0
5	1.8	1010	7.5	−4.9	52.8	0.0
6	2.9	850	—	−4.4	0	0.0
7	3.0	1000	17.75	−4.9	37.3	0.0
8	3.4	927	—	−4.8	0	0.0
9	3.8	1320	8.5	−5.3	45.1	0.0
10	4.4	890	—	−3.2	0	0.0
11	4.4	1065	22.5	−5.0	31.5	0.0
12	5.1	922	—	−3.3	0	−0.1
13	5.1	1116	10.5	−4.0	42.4	−0.2
14	5.7	1140	—	−4.6	0	−0.2
15	5.6	1355	12.0	−4.8	39.8	−0.2
16	6.6	1601	—	−3.8	0	−0.3
17	6.8	2054	15.75	−7.9	—	−0.3
18	7.7	2454	—	−3.3	0	−0.4
19	7.8	2651	20.25	−5.7	—	−0.4
20	9.1	3270	—	−2.1	0	−0.3
21	9.0	3463	11.75	−5.6	—	−0.5

performed in this study, water supercooling always preceded freezing. The cooling surface typically cooled to −5°C before freezing occurred. That is, $t_B(\tau)$ becomes negative during this period, as shown in Fig. 2(b). The regimes, in terms of R, are the same. However, in terms of the ambient water temperature, regions I, II, and III are defined by $t_\infty \leqslant 4$°C, $4 \leqslant t_\infty \leqslant 8 - t_B(\tau)$, and $t_\infty \geqslant 8 - t_B(\tau)$, respectively, assuming the density variation to be symmetric around t_m.

Table 1 contains some important data, including ambient water temperature t_∞, average abstracted heat flux before freezing $\overline{q''_{B,BF}}$ and maximum supercooling temperature at the cooling surface t_{msc}, for 21 representative experiments. A total of 67 experiments were performed. The flow visualizations of Fig. 3 are for experiment 2 of Table 1.

In Fig. 3(a), at $\tau \cong 4$ min, $t_B = -2.7$°C but freezing has not occurred. The flow is weak. Visual observation confirmed that the flow was upward. The characteristic velocity of the flow is estimated from the streak lengths to be 0.1 mm s^{-1}. Even though the upward buoyancy force represents a stable stratification, a flow has arisen. The fluid below the insulation on each side of the cooling surface initially has zero buoyancy force. Therefore, the pressure is lower there than it is immediately below the cooling surface, due to the upward buoyancy force in the developing thermal layer. This results in an outward flow. The asymmetry seen in the flow field may be due to small differences (about 0.1°C) in the cooling surface temperatures of the four quadrants. The flow is weak. It would be strongly affected by small bounding surface temperature differences.

As time progresses, the flow becomes stronger and a cellular pattern has developed, as shown in Figs. 3(b) and (c). The upward flow is now very near the surface and drives an inward downflow below it. The liquid is supercooled to $t_B = -4.5$ and −4.6°C in Figs. 3(b) and (c). The numerical value of $R(\tau)$ based upon $t_0 = t_{msc}$ is $R_{msc} = -0.57$. That is, the buoyancy force is everywhere upward.

In Fig. 3(d) ice has formed. The relevant value of $R(\tau)$, based upon $t_0 = t_{il} = 0$°C, is now $R_{ice} = -3.48$. This initial ice has a dendritic structure which may be inferred from the photograph. Immediately below the ice surface, the upflow has largely stagnated, but there is a weak out-flow near the edges, under the insulation. This is due to the dramatic decrease in the buoyancy force when ice forms.

The quantitative effect of ice formation on the buoyancy force may be assessed by defining a dimensionless buoyancy force parameter as

$$B(\tau) = \frac{\rho_\infty - \rho_0(\tau)}{\rho_m} \tag{2}$$

in terms of ρ, the fluid density. In equation (2), $\rho_0(\tau)$ is the density of the liquid at the bottom of the aluminum cooling surface, or if ice has formed, at the water–ice interface.

In Figs. 3(c) and (d), the buoyancy parameters are 4.7×10^{-4} and 1.5×10^{-4}, respectively. This is a 68% reduction due to the appearance of ice. Although the upflow below the cooling surface in Fig. 3(d) has ceased, the downflow continues, apparently due to its own inertia. The cellular pattern reappears in time, however, as seen in Fig. 3(e), although it is now much weaker. Notice that the ice retains a dendritic structure. This is because the ambient water temperature is close to 0°C. At higher water temperatures, the initial dendrites quickly disappear, leaving a flat, solid ice layer.

3.2. *Region* II: $0 \leqslant R \leqslant 1/2$

Figure 4 shows flow visualizations for an experiment at $t_\infty = 4.4°C$ (experiment 11, Table 1). In Fig. 4(a), at $\tau \cong 7$ min, a weak upflow has arisen, dominated by lateral effects at the edges. There are vortices near the edges of the cooling surface. The upflow has arisen because, as the aluminum surface is cooled, R decreases from an initially infinite value to one close to zero, near region I. Figure 4(b), at $\tau \cong 12$ min, shows that a returning downflow has arisen at the outer edges. The centerflow is still upward, and the value of R is 0.04. This is in region II and the downflow is expected to begin to dominate. This progresses in Fig. 4(c). The upflow becomes confined to a smaller region on the inside. Also notice the vortices just below the insulation near the edge of the cooling surface. The cell on the right-hand side turns clockwise. At the maximum supercooling temperature, $R_{msc} = 0.04$.

Figure 4(d) shows the time period in which freezing first occurs, so that $R_{ice} = 0.08$. This flow pattern had already arisen just before freezing. The flow is mostly downward, and the inside vortex on the left-hand side of Fig. 4(c) has disappeared, resulting in an asymmetric flow. In Fig. 4(e), the ice surface has become smooth. The flow moves downward with clockwise vortices at both the upper right and lower left edges of the plate. The estimated characteristic velocity is $U_c = 0.2$ mm s^{-1}.

Figure 5 shows the early flow evolution for $t_\infty = 5.6°C$ (experiment 15, Table 1). In Fig. 5(a), at $\tau \cong 1$ min, there is little flow, during the 20 s exposure time. In Fig. 5(b), motion has begun, in the form of pairs of vortices near the edges of the cooling surface. The outside vortex on the right turns counterclockwise. The vortices continue to grow as seen in Fig. 5(c). The outside vortices have become very much larger while the inside vortices have become somewhat larger and kidney shaped. The strong downflow on the outside has pushed the inside vortices away from the cooling surface. Figures 5(d) and (e) show the final stages of the flow development. The large downflows on the outside flank a central 'stagnant' region of upward buoyancy just below the center of the cooling surface. The characteristic velocity is $U_c = 0.6$ mm s^{-1}.

Figure 6 shows the continuing development of the flow, after $\tau \cong 10$ min, for the experiment of Fig. 5. Figure 6(a) is just before freezing. The stagnant region has decreased in size. Freezing occurred during the exposure of Fig. 6(b). The dendritic ice structure is again apparent. The stagnation region appears to have contracted, as R has increased from $R_{msc} = 0.15$ to $R_{ice} = 0.28$ with the appearance of ice. Figures 6(d) and (e) show the return of a large stagnant region under the ice. Notice also that the ice surface is smooth and flat, except at the edges.

3.3. *Region* III: $R \geqslant 1/2$

The visualizations for $t_\infty = 9.0°C$ (experiment 21, Table 1) are shown in Fig. 7. The condition at $\tau \cong 2.5$ min is shown in Fig. 7(a). A strong downflow, with $U_c = 0.8$ mm s^{-1}, has quickly developed. There are two small vortices below the center of the cooling surface. At this point $R(\tau) = 0.55$. Therefore, these vortices must be due to separation of the boundary layers from the cooling surface, rather than from density extremum effects. A few minutes later, in Fig. 7(b), the flow is essentially the same, but the vortices have grown. The cooling surface temperature is now $t_B = -4.1°C$, corresponding to $R(\tau) = 0.38$. Therefore, the instantaneous buoyancy force is now in region II, because of the liquid supercooling. Figure 7(c) shows well-defined vortices. They have increased in strength, perhaps due to the small upward buoyancy force near the cooling surface, now that the flow is in region II. Just before freezing, $R_{msc} = 0.34$.

In Fig. 7(d), ice has formed, and $R_{ice} = 0.55$. The ice was initially dendritic, but attained a solid form rather quickly. However, the ice surface is not flat. The small vortices appear to have decreased the local freezing rate in the two locations above the vortices, creating grooves in the water–ice interface. In our experiments, grooved ice also occurred at some of the higher water temperatures, in the range $4 \leqslant t_\infty \leqslant 8°C$. In Fig. 7(e), another set of grooves have appeared.

Figure 8 shows a photograph of the ice surface for the experiment of Fig. 7. The three-dimensionality of the flow is apparent from the grooves in both directions on the ice surface.

4. SENSOR MEASUREMENTS

Included in Table 1 are the ambient water temperature t_∞, average heat flux through the bottom of the aluminum cooling surface before freezing $\overline{q''_{B,BF}}$, and the time at which ice formed τ_{ice}. The maximum supercool temperature t_{msc}, ice formation efficiency E_{ice}, and tank bottom water temperature change during the experiment Δt_{TB}, are also included in the table. These quantities will be discussed in more detail in the following subsections.

Figures 9 and 10 contain time-dependent data for one non-freezing and one freezing experiment, respectively. Figure 9 (experiment 8, Table 1) shows data for abstracted heat flux from the bottom of the aluminum cooling surface $q''_B(\tau)$, aluminum cooling surface bottom temperature $t_B(\tau)$, heat transfer coefficient $h(\tau)$, and for $R(\tau)$. The instantaneous heat fluxes $q''_B(\tau)$ were calculated by using the measured temperatures in the aluminum cooling block to solve a transient, one-dimensional heat conduction problem using finite differences. The heat flux is very nearly constant, except for a starting transient. The scatter in $q''_B(\tau)$ is the result of uncertainties in the aluminum block temperatures.

The bottom cooling surface temperatures and the heat transfer coefficients at first decrease rapidly. They reach a steady level within about 15 min.

In Fig. 10 (experiment 9, Table 1), $q''_B(\tau)$, $t_B(\tau)$, $h(\tau)$, $R(\tau)$, and ice thickness $\delta(\tau)$ are shown. The jump in

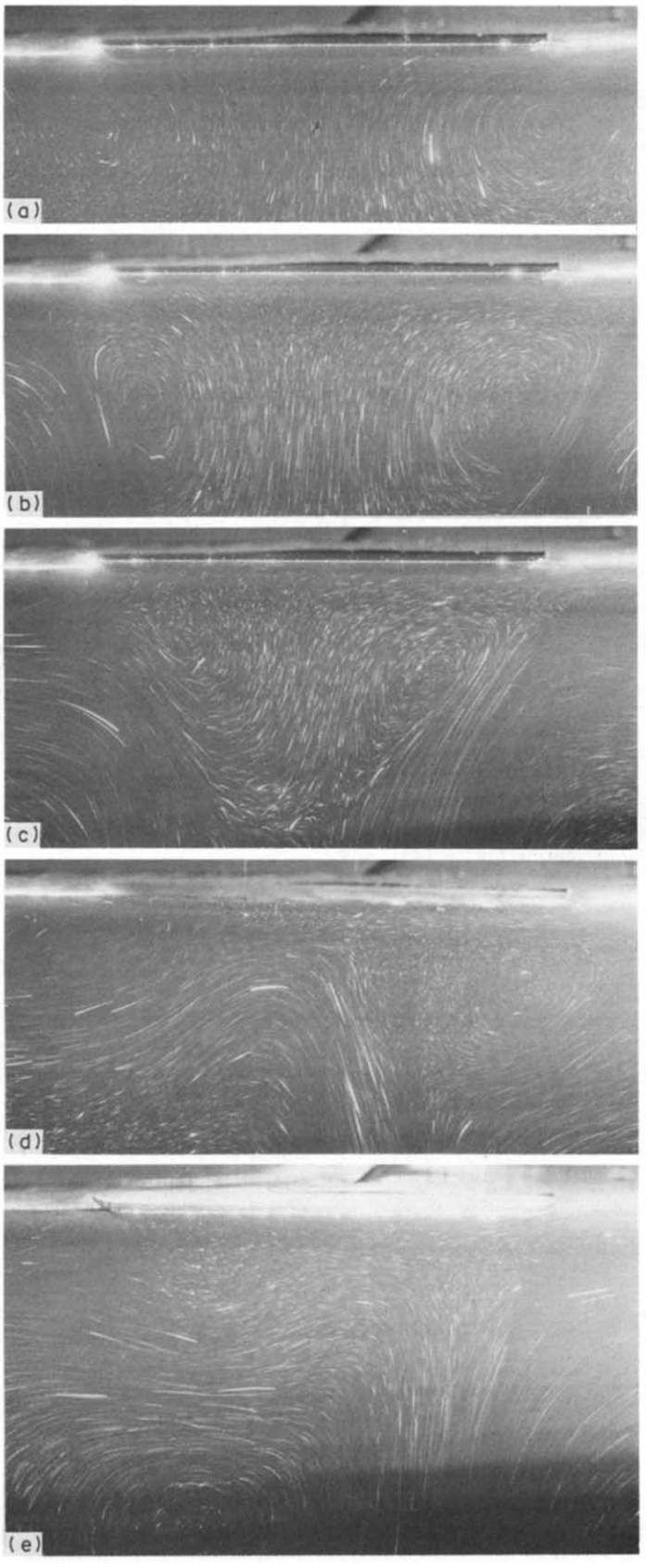

FIG. 4. Flow visualization for $t_\infty = 4.4°C$ and $\overline{q''_{B,BF}} = 1065\ W\ m^{-2}$. Exposure durations in seconds, effective surface temperatures, and R's are: (a) 380–440, −3.3°C, 0.05; (b) 700–760, −4.5°C, 0.04; (c) 940–1000, −4.8°C, 0.04; (d) 1340–1400, 0°C, 0.08; (e) 1740–1800, 0°C, 0.08.

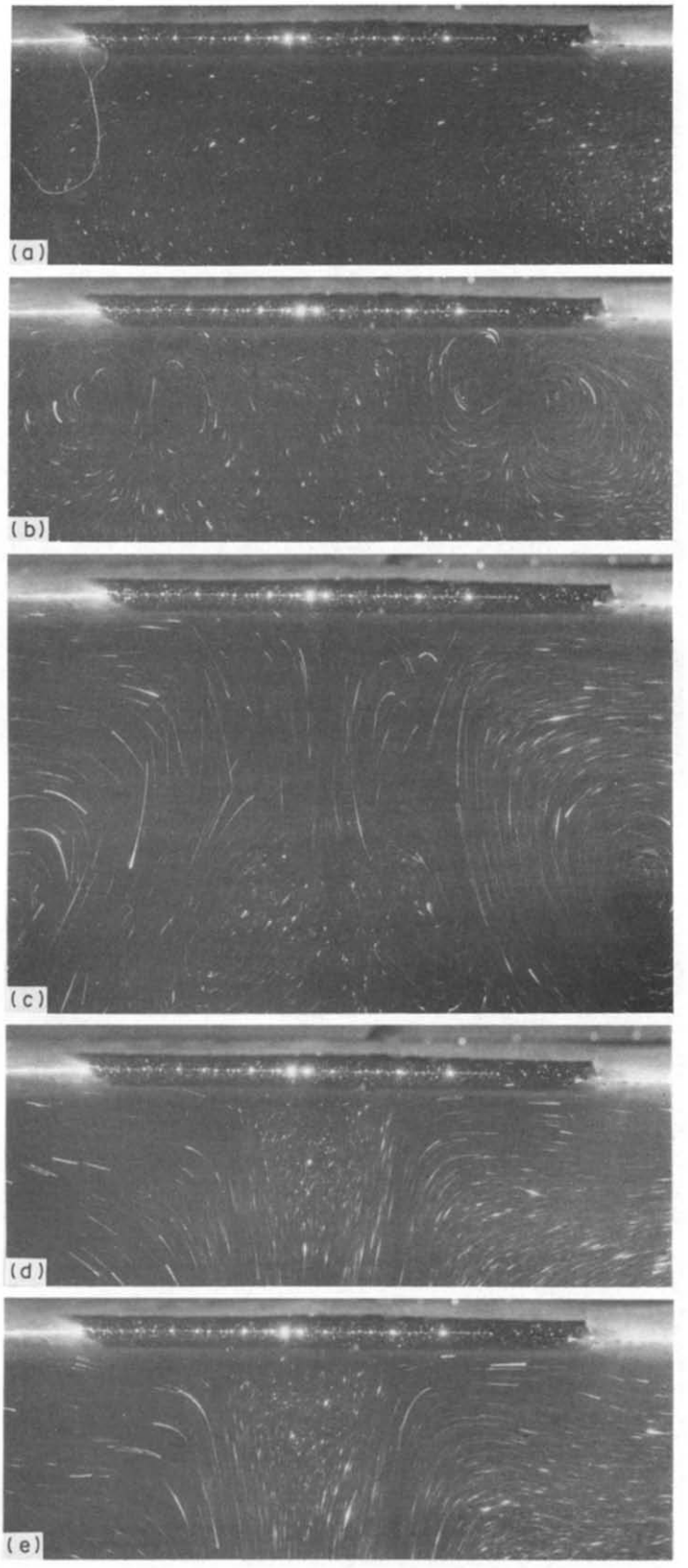

FIG. 5. Early development of a flow with $t_\infty = 5.6°C$ and $\overline{q''_{B,BF}} = 1355$ W m^{-2}. Exposure durations in seconds, effective surface temperatures and R's are: (a) 60–80, 2.4°C, 0.49; (b) 140–160, 0.3°C, 0.3; (c) 220–240, −1.2°C, 0.23; (d) 300–320, −2.4°C, 0.2; (e) 380–400, −3.1°C, 0.18.

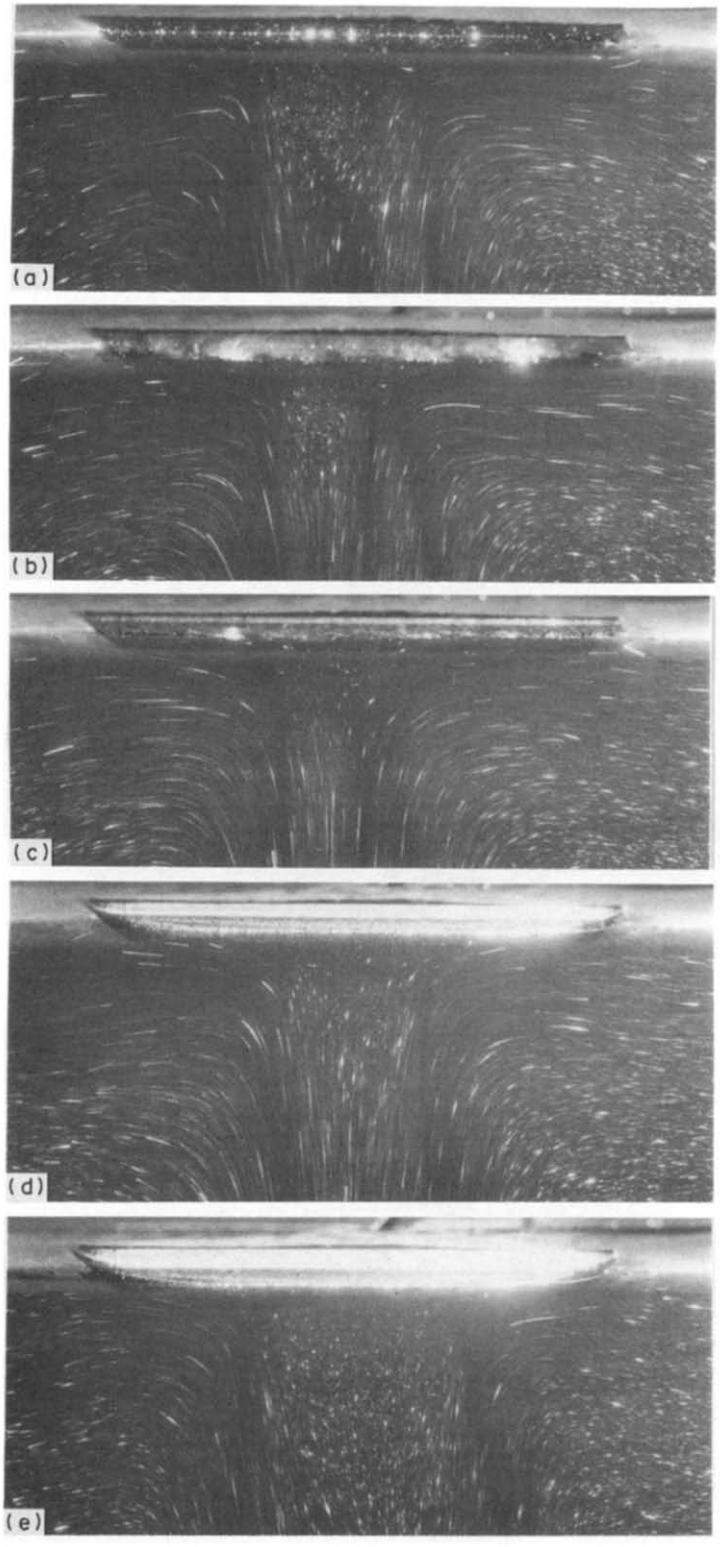

FIG. 6. Later development of a flow with $t_\infty = 5.6°C$ and $\overline{q''}_{B,BF} = 1355$ W m^{-2}. Exposure durations in seconds, effective surface temperatures, and R's are: (a) 620–640, −4.6°C, 0.15; (b) 700–720, −4.8°C, 0.15; (c) 780–800, 0°C, 0.28; (d) 1180–1200, 0°C, 0.28; (e) 1740–1760, 0°C, 0.28.

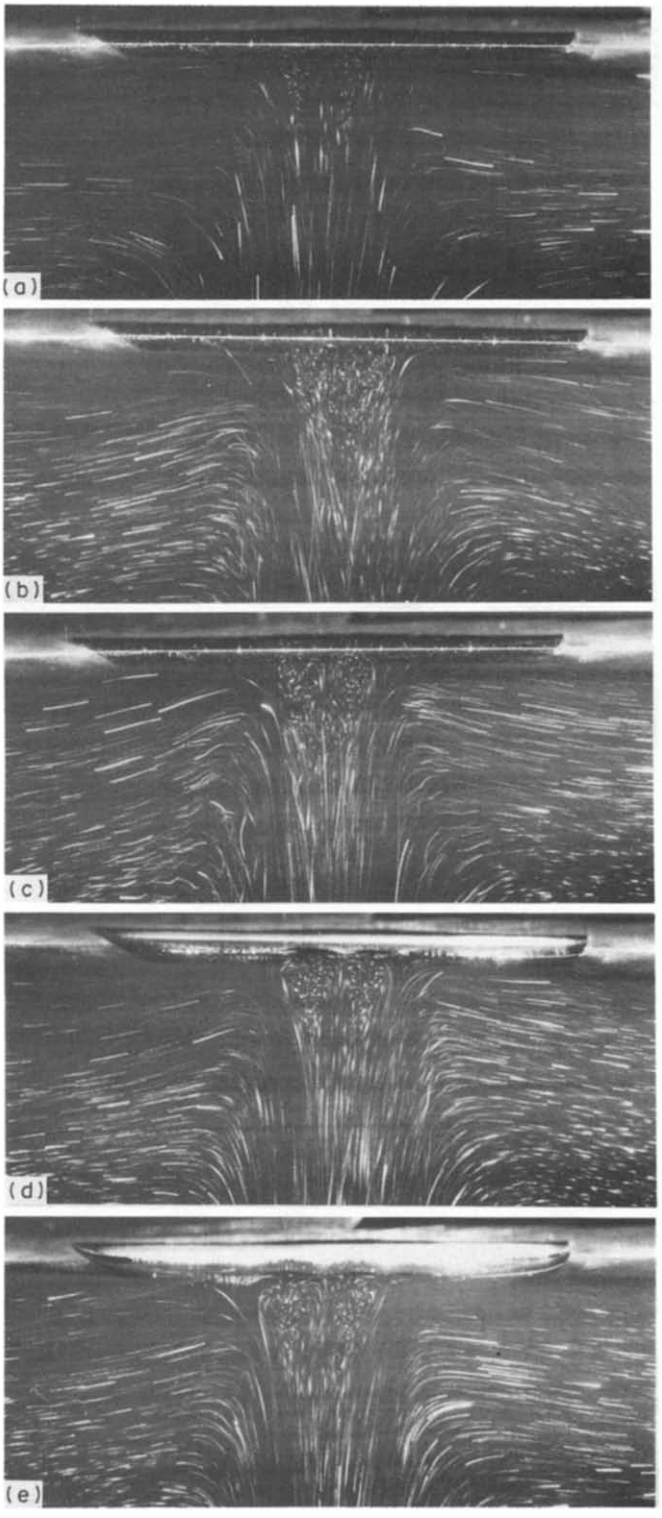

FIG. 7. Flow visualization for $t_\infty = 9.0°C$ and $\overline{q''}_{B,BF} = 3463\ W\ m^{-2}$. Exposure durations in seconds, effective surface temperatures, and R's are: (a) 135–150, −0.1°C, 0.55; (b) 360–375, −4.1°C, 0.38; (c) 660–675, −5.5°C, 0.34; (d) 885–900, 0°C, 0.55; (e) 1710–1725, 0°C, 0.55.

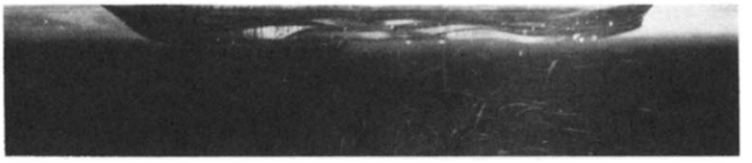

FIG. 8. Photograph of ice surface at end of experiment for $t_\infty = 9.0°C$ and $\overline{q''_{B,BF}} = 3463\ W\ m^{-2}$.

q''_B and t_B at $\tau = 8.5$ min marks the initial ice formation time. A large latent heat release occurs at the water–ice interface and $t_B(\tau)$ increases toward the equilibrium freezing temperature $t_{il} = 0°C$.

4.1. *Liquid supercooling*

As seen in Table 1, liquid supercooling always preceded freezing. Often, the liquid was cooled below $t_{il} = 0°C$, without freezing. Typically, freezing occurred when the cooling surface temperature t_B reached about $-5°C$, although some notable exceptions are seen. For example, in experiment 17, the cooling surface reached $-7.9°C$ before freezing, while in experiment 13, freezing occurred at $t_{msc} = -4.0°C$. On the other hand, in experiment 8, $t_{msc} = -4.8°C$, with no freezing.

The supercooling achieved in any particular experiment is a function of many variables, including water purity, cooling rate and physical condition of the cooling surface. Nucleation occurs on a microscopic level. The only control of the water condition was deionization to 0.1–0.5 MΩ cm. Since the critical

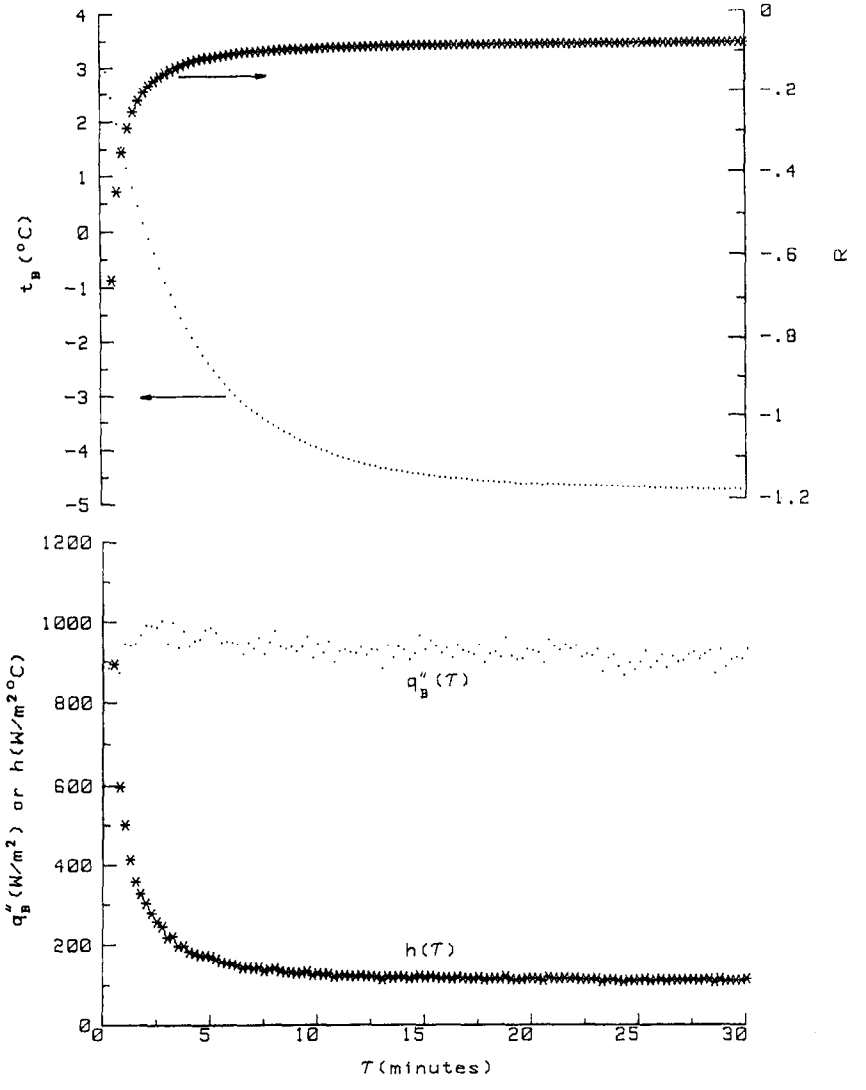

FIG. 9. Transient data for a non-freezing experiment with $t_\infty = 3.4°C$ and $\overline{q''_{B,BF}} = 927\ W\ m^{-2}$ (experiment 8, Table 1).

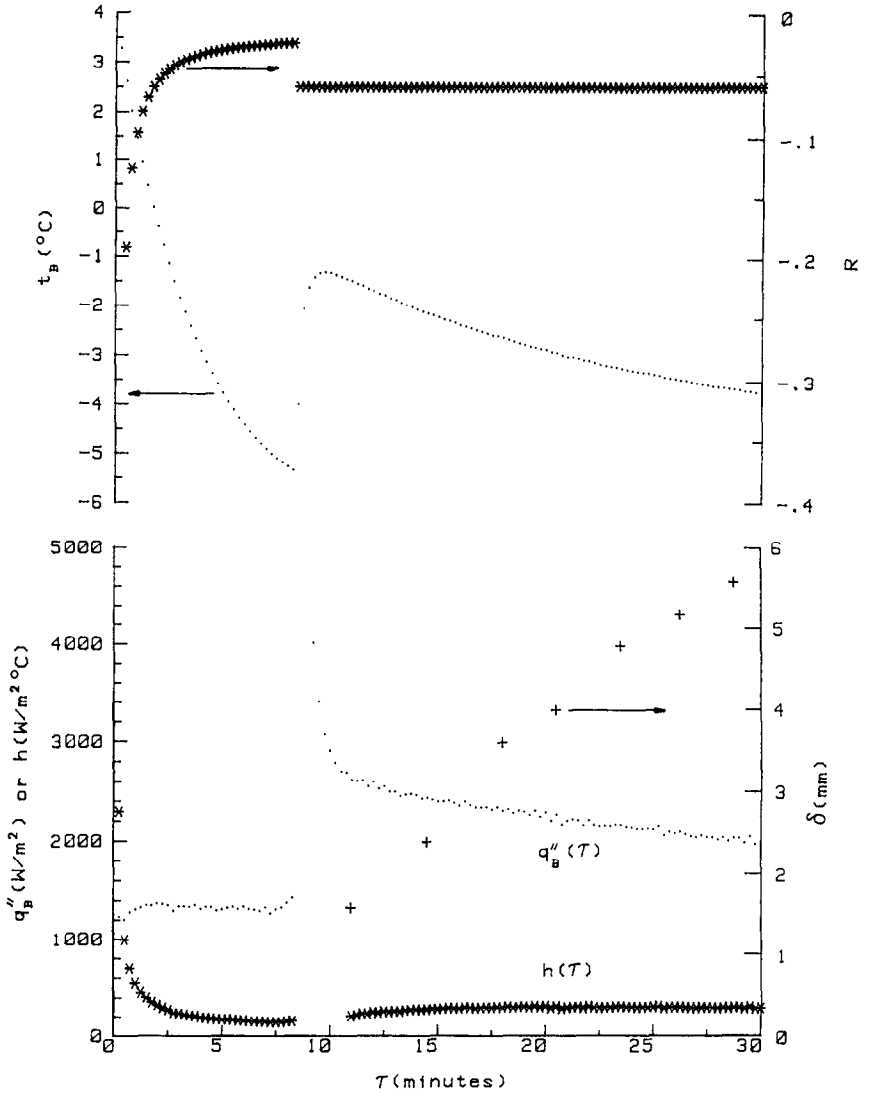

FIG. 10. Transient data for a freezing experiment with $t_\infty = 3.8°C$ and $\overline{q''_{B,BF}} = 1320$ W m^{-2} (experiment 9, Table 1).

radius for nucleation for 5°C supercooling was computed to be 0.01 μm, the pliolite particles do not account for the variability in the supercooling.

4.2. *Heat flux required for freezing*

The minimum heat flux for ice formation, as a function of ambient water temperature, is shown in Fig. 11. The asterisks are experiments in which freezing occurred, while the darkened circles are non-freezing experiments. The averaged heat fluxes before freezing were obtained by the formula

$$\overline{q''_{B,BF}} = \frac{1}{\tau_{ice}} \int_0^{\tau_{ice}} q''_B(\tau)\, d\tau \qquad (3)$$

where the integration was performed numerically using the trapezoidal rule. For non-freezing experiments, the upper limit of the integral was taken as $\tau = 30$ min.

An estimate of the dividing lines between freezing and non-freezing heat fluxes is also shown on Fig. 11. The crossover of some points is due to the variability in supercooling, as discussed above. Clearly, there is a large change in the slope of the two dividing lines near $t_\infty = 5.7°C$. This results from the change to a strong downflow from a weak upflow as the water increases above temperature t_m. This change in the nature of the flow was revealed in the flow visualizations of Section 3.

4.3. *Heat transfer coefficients*

Figure 12 shows the time variation of the heat transfer coefficients for five non-freezing experiments. When no ice is present, the instantaneous heat transfer coefficient is defined as

$$h(\tau) = \frac{q''_B(\tau)}{t_\infty - t_B(\tau)}. \qquad (4)$$

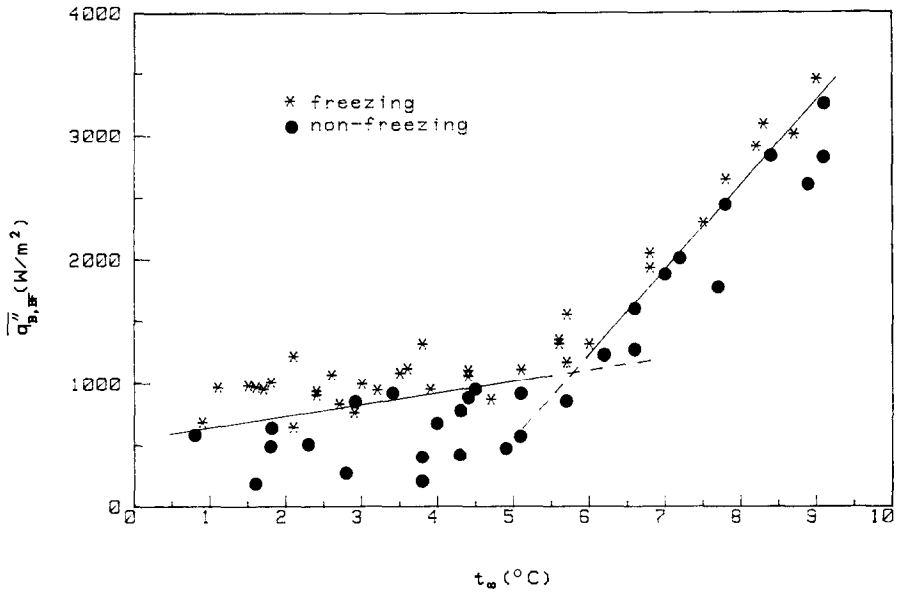

FIG. 11. Minimum heat flux required for freezing as a function of ambient water temperature.

It decreases rapidly from an initially very large value as the aluminum surface cools. A steady value is reached in about 10 min. Figure 12 shows that the ambient water temperature has almost no effect on the behavior of the convection heat transfer coefficient, in the temperature range $0.8 \leqslant t_\infty \leqslant 5.7°C$. However, for $t_\infty > 5.7°C$, the heat transfer coefficient increases with increasing ambient water temperature.

Steady heat transfer coefficients $\bar{h}$ for each non-freezing experiment were obtained by taking the arithmetic mean of $h(\tau)$ over the final 10 min, and are shown in Fig. 13. The circles represent experiments in which the aluminum surface was cooled to $-0.5 \leqslant t_B \leqslant 0.5°C$. The asterisks represent experiments in which significant supercooling occurred, $t_B \leqslant -2°C$.

An assessment of the effect of supercooling on the heat transfer coefficient was determined from this data. For water temperatures below $t_\infty \approx 5.7°C$, the heat transfer coefficients are higher for the experiments in which significant supercooling occurred because the supercooling increases the upward buoyancy force. Above $t_\infty \approx 5.7°C$, the experiments with significant supercooling have lower heat transfer coefficients because the downflow is opposed by an upward buoyancy force, due to supercooling effects. The overall trends are similar to Fig. 11, due to the change in the nature of the flow near $t_\infty = 5.7°C$.

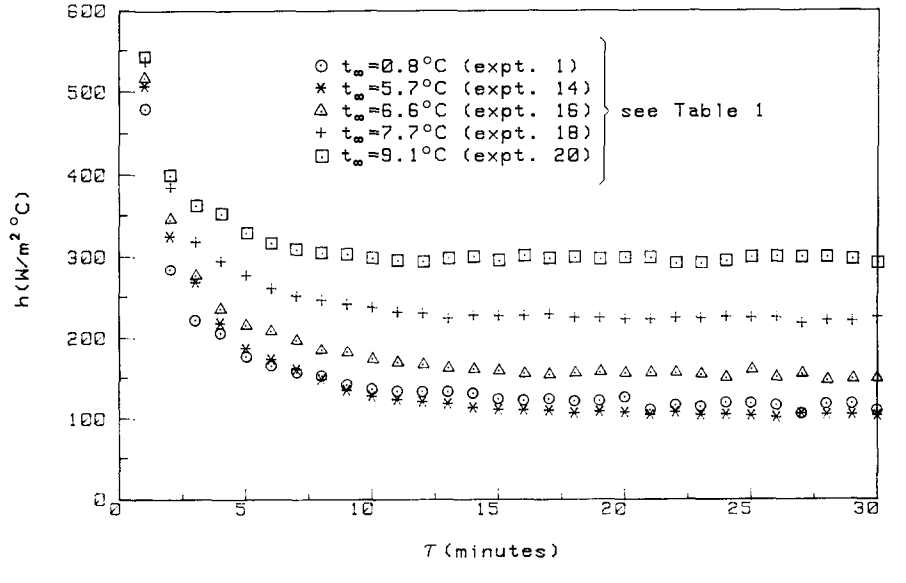

FIG. 12. Transient heat transfer coefficients for several non-freezing experiments.

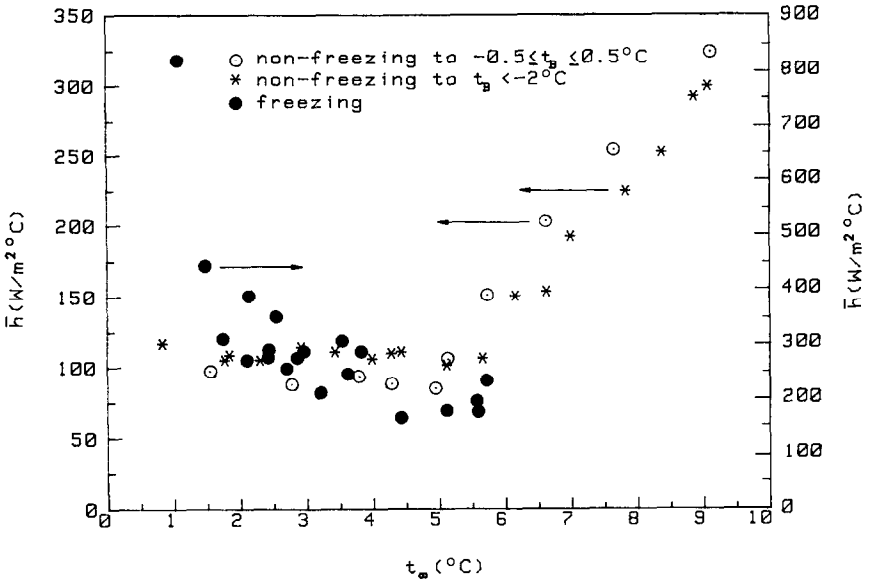

FIG. 13. Steady heat transfer coefficients, as a function of ambient water temperature t_∞.

Instantaneous values of $h(\tau)$ for five freezing experiments are shown in Fig. 14. Before freezing, the heat transfer coefficient is defined as above. After freezing, it is defined in terms of the convected heat flux $q''_{conv}(\tau)$, as

$$h(\tau) = \frac{q''_{conv}(\tau)}{t_\infty - t_{il}} \tag{5}$$

where

$$q''_{conv}(\tau) = q''_B(\tau) - q''_{ice}(\tau) \tag{6}$$

and

$$q''_{ice}(\tau) = \rho_{ice} h_{il} \frac{d\delta(\tau)}{d\tau} \tag{7}$$

is the rate of latent heat release due to ice formation per unit area of cooling surface, ρ_{ice} the density of ice, h_{il} the specific heat of fusion of water, and $\delta(\tau)$ the instantaneous ice thickness.

The ice growth rate $d\delta/d\tau$ was calculated by differentiating linear regression curve fits of the ice thickness data. The ice thickness function had the form

$$\delta(\tau) = K_0 + K_1(\tau - \tau_{ice})^p \tag{8}$$

where K_0, K_1, and p are constants defined by the curve fit. There is some justification for choosing a function of the above form, since analytical solutions of some conduction freezing problems yield

$$\delta(\tau) = C\tau^{1/2} \tag{9}$$

for freezing beginning at $\tau = 0$.

Figure 14 shows that the heat transfer coefficient

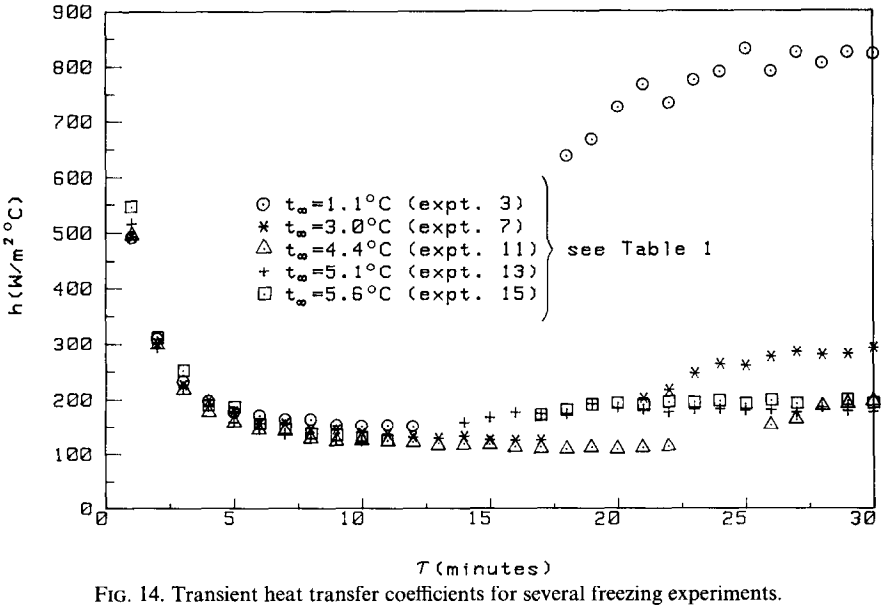

FIG. 14. Transient heat transfer coefficients for several freezing experiments.

rapidly decreases at the beginning of the experiment, as it did in the non-freezing experiments. The subsequent breaks in the data correspond to the beginning of freezing. No data is available immediately after initial ice formation, since the ice was dendritic and ice thickness measurements could not be made. Thereafter, however, $h(\tau)$ is higher than just before freezing. It continues to increase gradually, and typically reaches a steady value about 10 min after initial ice formation. The increase after ice formation arises since the relevant surface temperature increases from t_{msc} to $t_{il} = 0°C$. The convected heat flux $q''_{conv}(\tau)$ actually decreases after freezing, reflecting the decreased upward buoyancy force.

The 'steady' heat transfer coefficients after ice formation, as a function of ambient water temperature, are also shown in Fig. 13. These values were obtained by averaging $h(\tau)$ over the last 2 min of each experiment. Only results for experiments with $\tau_{ice} \leqslant 20$ min are given in Fig. 13. There is no data for $t_\infty > 5.7°C$ since all experiments performed at higher water temperatures resulted in 'grooved' ice and no accurate calculation for $q''_{ice}(\tau)$ could be made.

4.4. *Ice formation efficiencies*

The ice formation efficiency, E_{ice}, is defined as the percentage of heat transferred through the cooling surface which results from latent heat release, over the course of the 30 min experiment. This is expressed as

$$E_{ice} = \frac{Q_{ice}}{Q_B} \times 100 \tag{10}$$

where

$$Q_{ice} = A\rho_{ice}h_{il}\delta(\tau = 30\,\text{min}) \tag{11}$$

$$Q_B = A\int_0^{30\,\text{min}} q''_B(\tau)\,d\tau \tag{12}$$

and A is the area of the aluminum cooling surface.

From Table 1, E_{ice} typically ranges from 35 to 50%. There is no obvious trend to the data, since E_{ice} is dependent upon the level of supercooling and on the time at which freezing begins.

4.5. *Ambient fluid stratification*

The last column of Table 1 contains the measured water temperature changes at the bottom of the tank over the length of each experiment Δt_{TB}. This indicates the importance of the ambient fluid stratification which arises. This effect is not important for the experiments with $t_\infty \leqslant 4°C$, which are characterized by weak upflows. For strong downflows at higher water temperatures, however, the tank bottom temperature decreases by as much as 0.5°C, indicating significant ambient stratification during the experiment.

5. CONCLUSIONS

Time-exposure photographs of flow, and temperature and ice thickness measurements have been used to examine the thermal and fluid flow processes associated with the downward freezing of pure water from above. For low ambient water temperatures, $t_\infty \leqslant t_m$, the flow is initially weak and upward. It later develops into a cellular pattern. Water supercooling and subsequent freezing has a large effect on these flows because the transient buoyancy force is greatly reduced in magnitude after ice forms. Ambient fluid stratification is not an important effect in region I.

For somewhat higher water temperatures (region II), the flows which arise may be very complicated due to buoyancy force reversals. For $t_\infty = 4.4°C$, the flow was very complex, but was dominated by the downward buoyancy force. Reduction of the buoyancy force with freezing did not produce the significant effects seen in region I. For $t_\infty = 5.6°C$, the flow was mostly downward with a stagnated region below the center of the cooling surface. This region results from a locally upward buoyancy force. At this water temperature, ambient fluid stratification became important.

For ambient water temperatures in region III, the flow was downward, except for two continuing small vortices below the center of the cooling surface. These vortices are thought to result from separation of the boundary layers from the cooling surface. The water–ice interface was grooved, due to reduction of the local freezing rate by the vortices.

In general, the flows before and after freezing may be characterized by the parameters R_{msc} and R_{ice}, respectively. In conditions wherein freezing occurred, the water was supercooled to $t_{msc} \approx -5°C$. After freezing, the bottom surface temperature is about 0°C. This change in the surface temperature changes the buoyancy force strength and qualitative features of the flow.

The minimum heat flux required to achieve freezing for ambient water temperatures between 1 and 9°C has been determined. Below $t_\infty \cong 5.7°C$, this required heat flux increases gradually with increasing water temperature. However, it increases much more rapidly for $t_\infty > 5.7°C$.

Convective heat transfer coefficients during freezing experiments increase with the onset of freezing. This arises as the effective surface temperature increases from t_{msc} to t_{il}. However, the convected heat flux from the water to the phase interface decreases with freezing. The measured heat transfer coefficients reported in this paper are believed to be the first for downward freezing into a deep body of pure water.

Acknowledgements—The authors acknowledge support for this research through NSF grant CBT 84 18517 and through the Gabel Fund at the University of Pennsylvania.

REFERENCES

1. Y. Joshi and B. Gebhart, Measurements and visualizations of transient and steady-state vertical natural

convection flow in cold water, *Int. J. Heat Mass Transfer* **29,** 1723–1740 (1986).
2. B. Sammakia and B. Gebhart, Transport near a vertical ice surface melting in water of various salinity levels, *Int. J. Heat Mass Transfer* **26,** 1439–1452 (1983).
3. L. J. Thomas and J. W. Westwater, Microscopic study of solid–liquid interfaces during melting and freezing, *Chem. Engng Prog. Symp. Ser.* **59**(41), 155–164 (1963).
4. D. V. Boger and J. W. Westwater, Effect of buoyancy on the melting and freezing processes, *Trans. Am. Soc. Mech. Engrs*, Series C, *J. Heat Transfer* **89,** 81–89 (1967).
5. T. D. Foster, Experiments on haline convection induced by the freezing of sea water, *J. Geophys. Res.* **74,** 6967–6974 (1969).
6. R. S. Tankin and R. Farhadieh, Effects of thermal convection currents on formation of ice, *Int. J. Heat Mass Transfer* **14,** 953–961 (1971).
7. R. Farhadieh and R. S. Tankin, Interferometric study of freezing of sea water, *J. Geophys. Res.* **77,** 1647–1657 (1972).
8. R. Farhadieh and R. S. Tankin, A study of the freezing of sea water, *J. Fluid Mech.* **71,** 293–304 (1975).
9. B. W. Grange, R. Viskanta and W. H. Stevenson, Diffusion of heat and solute during freezing of salt solutions, *Int. J. Heat Mass Transfer* **19,** 373–384 (1976).
10. B. W. Grange, R. Viskanta and W. H. Stevenson, Interferometric observation of thermohaline convection during freezing of saline solution, *Lett. Heat Mass Transfer* **4,** 85–92 (1977).
11. C. Gau and R. Viskanta, Flow visualization during solid–liquid phase change heat transfer, I. Freezing in a rectangular cavity, *Int. Commun. Heat Mass Transfer* **10,** 173–181 (1983).
12. T. Nishimura, S. Ito, H. Tsuboi and Y. Kawamura, Analysis of two-dimensional freezing by the finite-element method, *Int. Chem. Engng* **25,** 105–112 (1985).
13. B. Gebhart, M. S. Bendell and H. Shaukatullah, Buoyancy induced flows adjacent to horizontal surfaces in water near its density extremum, *Int. J. Heat Mass Transfer* **22,** 137–149 (1979).
14. B. Gebhart and J. C. Mollendorf, A new density relation for pure and saline water, *Deep-Sea Res.* **24,** 831–848 (1977).
15. J. C. Mollendorf and K. H. Jahn, Onset of convection in a horizontal layer of cold water, *Trans. Am. Soc. Mech. Engrs*, Series C, *J. Heat Transfer* **105,** 460–464 (1983).

ETUDE EXPERIMENTALE DES EFFETS DE CONVECTION NATURELLE SUR LA CONGELATION DESCENDANTE D'EAU PURE

Résumé—On présente des mesures de congélation descendante dans une couche profonde d'eau pure. Ceci se rencontre dans les procédés et sur les bassins d'eau terrestres. Les mécanismes couplés de convection et de congélation sont très compliqués, dus à l'antagonisme du transport thermique d'eau froide et du sous-refroidissement du liquide. Des études antérieures comparables ont été limitées à des géométries petites et très confinées. Les mesures à grande échelle présentées ici déterminent à la fois les flux de congélation et le transfert thermique convectif. On donne des visualisations chronologiques d'écoulements typiques pour des températures ambiantes d'eau dans le domaine 1–9°C. L'anomalie de densité de l'eau froide a un effet très important sur les écoulements et les flux de congélation. Un grand sous-refroidissement du liquide précède toujours le début de la congélation. Des changements transitoires dans la force d'Archimède ont des effets importants. Des mesures des épaisseurs de glace et des températures de surface froide sont utilisées pour calculer les coefficients de transfert thermique et les "efficacités" de croissance de glace. Ces mesures fournissent des renseignements quantitatifs détaillés sur les rôles relatifs du sous-refroidissement, de la congélation et de la convection naturelle dans les mécanismes de descente de la surface de glace horizontale dans l'eau froide.

EXPERIMENTELLE UNTERSUCHUNG DER NATÜRLICHEN KONVEKTION BEI DER ABWÄRTSGERICHTETEN EISBILDUNG IN REINEM WASSER

Zusammenfassung—Es werden Messungen bei der abwärtsgerichteten Eisbildung in einer ruhenden, tiefen, reinen Wasserschicht vorgestellt. Dies kommt sowohl bei technischen Prozessen als auch in der Natur vor. Die gekoppelten Mechanismen von Konvektion und Eisbildung sind sehr komplex, bedingt durch das Auftreten des Dichtemaximums von Wasser und durch die Flüssigkeitsunterkühlung. Frühere vergleichbare Untersuchungen beschränken sich auf kleine und begrenzte Abmessungen. Die gegenwärtigen umfangreichen Messungen bestimmen sowohl die durch das Gefrieren als auch durch Konvektion übertragenen Wärmeströme. Es wurden auch Messungen ohne Gefriervorgang durchgeführt, um den reinen Konvektionseinfluß zu charakterisieren. Aufnahmen von typischen Strömungen für Wassertemperaturen im Bereich 1 bis 9°C werden vorgelegt. Die Dichteanomalie des kalten Wassers hat einen sehr ausgeprägten Einfluß auf die Strömungen und Gefriergeschwindigkeiten. Dem Gefrierbeginn geht immer eine große Flüssigkeitsunterkühlung voraus. Die transienten Änderungen der Auftriebskraft haben einen großen Einfluß. Messungen der Eisdicken und Kühloberflächentemperaturen werden zur Berechnung der Wärmeübergangskoeffizienten und der Eiswachstums-Effizienz benutzt. Diese Messungen liefern einen detaillierten quantitativen Einblick in die jeweilige Rolle von Unterkühlung, Gefriervorgang und natürlicher Konvektion bei horizontalen, an der Unterseite zunehmenden Eisschichten in kaltem Wasser.

ЭКСПЕРИМЕНТАЛЬНОЕ ИЗУЧЕНИЕ ВЛИЯНИЯ ЕСТЕСТВЕННОЙ КОНВЕКЦИИ НА ПРОМЕРЗАНИЕ СЛОЯ ЧИСТОЙ ВОДЫ

Аннотация—Представлены результаты измерения процесса промерзания гдубокого слоя покоящейся чистой воды. Данное явление имеет место как в технологических процессах, так и в природе. Показано, что взаимодействие конвекции и замерзания очень сложно как из-за своеобразного поведения подъемной силы, определяющей теплоперенос в холодной воде, так и вследствие переохлаждения жидкости. Ранее проведенные сравнительные исслодования проводились в малых объемах весьма ограниченных геометрий. По данным настоящих измерений, выполненных на увеличенных масштабах, найдены интенсивности замерзания и конвективного теплопереноса. Чтобы выделить чисто конвективные эффекты, проведены также измерения в отсутствие процесса замерзания. Наблюдения в отдельные моменты времени типичных течений выполнены в интервале температуры окрухающей воды 1–9°C. Аномалия плотности в холодной воде оказывает сильное влияние как на интенсивность конвекции, так и на скорость замерзания. Сильное переохлаждение жидкости всегда предшествует начальной стадии замерзания. Найдено, что влияние немонотонного изменения плотности во многих случая велико. По результатам измерений толщины льда и температуры охлаждающих поверхностей рассчитаны коэффициенты теплопереноса и 'производительность' роста льда. Данные измерения позволяют детально количественно сценить относительные роли переохлаждения воды, замерзания и естественной конвекции в процессах образования горизонтальных поверхностей льда в холодной воде.